Acta Crystallographica Section D
Biological Crystallography
ISSN 0907-4449

Structure of T4moC, the Rieske-type ferredoxin component of toluene 4-monooxygenase

Luke A. Moe,[a] Craig A. Bingman,[b] Gary E. Wesenberg,[b] George N. Phillips Jr[a,b] and Brian G. Fox[a,b]*

[a]Department of Biochemistry, University of Wisconsin–Madison, USA, and [b]Center for Eukaryotic Structural Genomics, University of Wisconsin–Madison, USA

Correspondence e-mail: bgfox@biochem.wisc.edu

Received 5 December 2005
Accepted 17 February 2006

PDB Reference: T4moC, 1vm9, r1vm9sf.

The structure of the Rieske-type ferredoxin (T4moC) from toluene 4-monooxygenase was determined by X-ray crystallography in the $[2Fe–2S]^{2+}$ state at a resolution of 1.48 Å using single-wavelength anomalous dispersion phasing with the [2Fe–2S] center. The structure consists of ten β-strands arranged into the three antiparallel β-sheet topology observed in all Rieske proteins. Trp69 of T4moC is adjacent to the [2Fe–2S] centre, which displaces a loop containing the conserved Pro81 by ~8 Å away from the [2Fe–2S] cluster compared with the Pro loop in the closest structural and functional homolog, the Rieske-type ferredoxin BphF from biphenyl dioxygenase. In addition, T4moC contains five hydrogen bonds to the [2Fe–2S] cluster compared with three hydrogen bonds in BphF. Moreover, the electrostatic surface of T4moC is distinct from that of BphF. These structural differences are identified as possible contributors to the evolutionary specialization of soluble Rieske-type ferredoxins between the diiron monooxygenases and *cis*-dihydrodiol-forming dioxygenases.

1. Introduction

Rieske [2Fe–2S] clusters have a metal-binding motif of Cys-Xaa-His and Cys-Xaa-Xaa-His separated by 15–21 amino acids, where the SG atoms of the two Cys residues bind one Fe atom and the ND1 atoms of the two His residues bind the other Fe atom. This motif is found in membrane oxidase complexes (Berry *et al.*, 2000), *cis*-dihydrodiol-forming aromatic dioxygenases (Batie *et al.*, 1992), bacterial nitrite reductases (Harborne *et al.*, 1992) and arsenite oxidases (Ellis *et al.*, 2001). Rieske-type ferredoxins are also found as soluble electron carriers in some *cis*-dihydrodiol-forming aromatic dioxygenases (Batie *et al.*, 1992) and in some diiron monooxygenases (Leahy *et al.*, 2003). Structures of these ferredoxins have been determined by X-ray crystallography (Iwata *et al.*, 1996; Berry *et al.*, 1999; Carrell *et al.*, 1997; Hunsicker-Wang *et al.*, 2003; Bonisch *et al.*, 2002; Kauppi *et al.*, 1998; Martins *et al.*, 2005; Ellis *et al.*, 2001; Colbert *et al.*, 2000; Nam *et al.*, 2005) and NMR (Skjeldal *et al.*, 2004).

Toluene 4-monooxygenase is a diiron monooxygenase complex that catalyzes the NADH- and O_2-dependent hydroxylation of toluene to form *p*-cresol (Pikus *et al.*, 1996). This enzyme consists of a diiron hydroxylase, an oxidoreductase, a catalytic effector protein and a 112-amino-acid Rieske-type ferredoxin (T4moC). Here, we report the X-ray structure of T4moC from *Pseudomonas mendocina* KR1, determined in the oxidized state at a resolution of 1.48 Å.

2. Materials and methods

2.1. Materials

The GenBank accession number for the T4moC gene is gi:45479223 (Yen *et al.*, 1991). The T4moC residues Cys84 and Cys85 were mutated to Ala using pRS184f (Studts *et al.*, 2000) as a template using the QuikChange II kit (Stratagene, La Jolla, CA, USA). Vent DNA polymerase and restriction enzymes were from New England Biolabs (Beverly, MA, USA). Turbo and Yield Ace DNA polymerases were from Stratagene. DNA extraction and purification kits were from Q-BIO (Carlsbad, CA, USA) and Qiagen (Valencia, CA, USA). *Escherichia coli* strains DH5α (Pharmacia, Piscataway, NJ, USA), NovaBlue and BL21 (DE3) (Novagen, Madison, WI, USA) were used for cloning and expression, respectively. PCR primers were from Integrated DNA Technologies, Inc. (Coralville, IA, USA). Methods for expression and purification of the doubly mutated T4moC were the same as for the native ferredoxin (Xia *et al.*, 1998). The reconstitution of the purified T4MO complex and determination of catalytic activity with the mutated T4moC were also as previously described (Mitchell *et al.*, 2002).

2.2. Crystallization

T4moC ($\sim$20 mg ml^{-1}) was dialyzed in 25 m*M* HEPES pH 7.0 containing 25 m*M* NaCl for 20 h at 277 K prior to crystallization trials. Crystals grew as brown plates from a light precipitate at 293 K from a hanging drop containing 10 mg ml^{-1} protein, 0.100 *M* MES acetate pH 6.0, 0.16 *M* magnesium chloride and 24%(*w*/*v*) MePEG 5000. Crystals were flash-frozen in the crystallization mother liquor plus 15% ethylene glycol after an incubation time of 10 s using liquid N_2.

2.3. Structure determination

A single-wavelength anomalous diffraction data set extending to 1.89 Å was collected from a cryopreserved crystal on an R-AXIS IV detector using Cu $K\alpha$ radiation from a Rigaku RU-200 rotating-anode generator with Osmic multilayer optics. A second data set extending to 1.48 Å was collected at 0.97924 Å at Sector 32 of the Advanced Photon Source. Diffraction data were reduced and scaled using *HKL*2000 (Otwinowski & Minor, 1997). Two iron sites per asymmetric unit were located using the Cu $K\alpha$ data set and *SnB*. The structure was phased using *SOLVE*/*RESOLVE* (Terwilliger, 2002) and phases were extended to the high-resolution data set using *ARP*/*wARP* (Terwilliger, 2003). The initial model comprised 103 residues in two chains, with side chains docked to all residues. The structure was completed using alternative cycles of map fitting in *XFIT* (McRee, 1999) and refinement in either *CNS* (Brünger *et al.*, 1998) or *REFMAC* 5.1.24 (Murshudov *et al.*, 1997).

2.4. Other analyses

The *APBS* program (Baker *et al.*, 2001) and the Amber02 force field were used to calculate surface electrostatic potentials by the nonlinear Poisson–Boltzmann method (Holst & Saied, 1995). The cysteine ligands were assigned the CYM residue type, the histidine ligands were assigned the HIE residue type (consistent with the protonation state assigned by

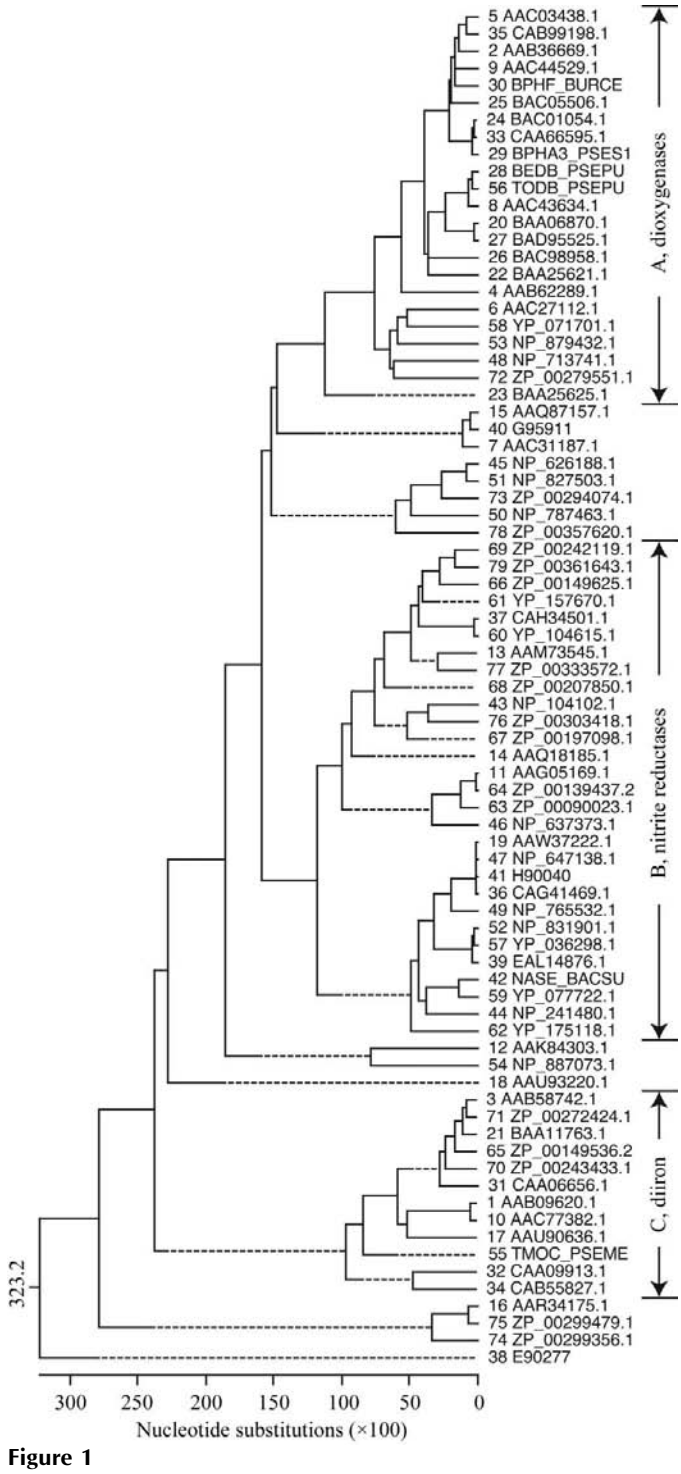

Figure 1
Rooted cladogram of Rieske-type ferredoxins obtained from alignment by *CLUSTAL W*. Three clades associated with known functions are reported: A, Rieske-type ferredoxins from *cis*-dihydrodiol-forming aromatic dioxygenases; B, subunits of bacterial assimilatory nitrite reductase; C, Rieske-type ferredoxins from bacterial diiron monooxygenases. Ferredoxins described in the text are T4moC, TMOC_PSEME; TbuB, AAB09620.1; BphF, BPHF_BURCE; CarAc, the Rieske-type ferredoxin of the carbazole 1,9a-dioxygenase, BAA21733.

Table 1
Summary of data-collection, crystal structure and refinement statistics for 1vm9.

Values in parentheses are for the highest resolution shell.

Space group	$C222_1$†	$C222_1$‡
Wavelength (Å)	1.5418	0.97924
Unit-cell parameters	a = 44.353, b = 52.360, c = 83.476	a = 44.360, b = 52.530, c = 83.490
Resolution range (Å)	33.84–1.89 (1.96–1.83)	33.92–1.48 (1.52–1.48)
Unique/total reflections	8069/85087	16626/225464
Completeness (%)	99.5 (95.2)	99.9 (99.8)
Redundancy	10.5 (8.0)	13.6 (11.8)
$R_{\rm merge}$	0.060 (0.210)	0.055 (0.277)
Mean $I/\sigma(I)$§	20.63 (8.31)	32.45 (7.75)
Mean figure of merit (*SOLVE*)	0.32	
Non-H atoms¶		996
Solvent molecules††		138
R value (working set + test set)‡‡		0.156
R value (working set)§§		0.155 (0.196)
Free R value¶¶		0.176 (0.213)
Mean B value (Å^2)		14.04
Ramachandran analysis (%)		
Most favored		91.3
Additionally allowed		8.7
R.m.s. deviation of refined atoms		
Bond lengths (Å)		0.020
Bond angles (°)		2.427

† Data collected at UW. ‡ Data collected at Sector 32 of the Advanced Photon Source. § The root-mean-squared value of the intensity measurements divided by their estimated standard deviation. ¶ Number of non-H atoms included in refinement. †† These include two Mg atoms, three ethylene glycol molecules and 133 water molecules. ‡‡ $R_{\rm sym} = \sum |I - \langle I\rangle|/\sum I$, where I is the observed intensity and $\langle I\rangle$ is the average intensity obtained from multiple measurements. §§ R value = $\sum ||F_{\rm o}| - |F_{\rm c}||/\sum |F_{\rm o}|$, where $|F_{\rm o}|$ is the observed structure-factor amplitude and $|F_{\rm c}|$ is the calculated structure-factor amplitude. ¶¶ $R_{\rm free}$ = R factor based on 5.1% of the data excluded from refinement.

NMR; Skjeldal *et al.*, 2004) and a simple [2Fe–2S] cluster core was assigned consisting of two Fe^{3+} ions and two S^{2-} ions. The protein dielectric was 2 and the solvent dielectric was 80. PFAM searches were performed at the Washington University mirror site (http://pfam.wustl.edu). The primary sequences of Rieske [2Fe–2S] domains were obtained from a *BLASTP* 2.2.11 (Altschul *et al.*, 1997) search initiated at http://www.dnastar.com/blast/ncbi-blast.html using the T4moC primary sequence as the query and the BLOSUM62 matrix. After removal of redundant sequences, multiple sequence alignments and rooted cladograms were produced from the *MegAlign* module of *LASERGENE* (v.5.52, DNAStar, Madison, WI, USA) using *CLUSTAL W* (Higgins *et al.*, 1996) with a gap penalty of 10.00, a gap length of 0.2 and the BLOSUM protein weight matrix. The *CLUSTAL W* primary sequence alignment was modified to correspond to the residue positions observed in the loops of the aligned structures of each ferredoxin. The *VAST* website (http://www.ncbi.nlm.nih.gov/Structure/VAST/vastsearch.html) was used to identify structurally related proteins in the Molecular Modeling Database (Chen *et al.*, 2003). *ESyPred3D* (Lambert *et al.*, 2002) was used for molecular threading of TbuB, the Rieske-type ferredoxin of the toluene monooxygenase complex from *Ralstonia pickettii* PK01 (GenBank AAB09620.1), to the T4moC structure (PDB code 1vm9). Figures were created with *PyMOL* (DeLano Scientific LLC, Castro City, CA, USA).

3. Results and discussion

3.1. Phylogenetic relationships

The Rieske [2Fe–2S] domain is assigned to PFAM domain PF00355. A *BLASTP* search using the complete T4moC protein sequence gave 79 non-redundant sequences with a length of 95–134 amino acids, a maximum gap of two over the central core of ~80 amino acids and E-value probability scores between 7×10^{-63} and 0.001. These restrictions excluded the Rieske [2Fe–2S] domains from the membrane oxidase complexes, the *cis*-dihydrodiol dioxygenases and the arsenite oxidases.

Fig. 1 shows the rooted cladogram calculated from alignment of these sequences along with the identities of each sequence. The functions associated with the major clades are A, Rieske-type ferredoxin components of *cis*-dihydrodiol-forming aromatic ring dioxygenases, B, small subunits of assimilatory nitrite reductases, and C, Rieske-type ferredoxin components of diiron hydroxylase enzymes. While the sequence identity within each of the major clades is relatively high (15–98% for nitrite reductase subunits; 21–96% for the aromatic dioxygenase ferredoxins; 23–98% for the diiron hydroxylase ferredoxins), the identity between the clades is significantly lower (~15–21%). A primary sequence alignment for T4moC, TbuB and BphF is given as supplementary material[1]. Other minor clades and singletons shown in the cladogram were annotated to be electron carriers for aromatic ring dioxygenases or to be uncharacterized ferredoxins or hypothetical proteins.

The Rieske ferredoxins known to act as intermediary electron carriers for the diiron hydroxylase superfamily were clustered into the same clade, which implies evolutionary specialization with an ancestral diiron hydroxylase. A similar possibility has been discussed for the evolution of diiron hydroxylase effector proteins toward their known catalytic specializations (Coufal *et al.*, 2000; Hemmi *et al.*, 2001; Mitchell *et al.*, 2002) and reviewed for the entire diiron hydroxylase superfamily (Leahy *et al.*, 2003). Likewise, the evolutionary specialization of the ferredoxins of the *cis*-dihydrodiol-forming aromatic dioxygenases has been considered in detail by others (Batie *et al.*, 1992; Nam *et al.*, 2001).

3.2. Crystallization

Aerobic crystallization trials with natural T4moC gave progressive aggregation and bleaching. As neither Cys84 nor Cys85 was conserved in the Rieske-type ferredoxins from other diiron hydroxylases and since these residues were likely to be surface-exposed (Skjeldal *et al.*, 2004), they were changed to Ala. The doubly mutated protein was prepared by the same procedures used for the natural ferredoxin. When

[1] Supplementary material has been deposited in the IUCr electronic archive (Reference: BE5051). Details for accessing this material are given at the back of the journal.

included in standard assays, it gave comparable catalytic activity and regiospecificity for toluene oxidation by the T4MO complex as the natural T4moC. The mutated T4moC was used in crystallization trials and the crystals obtained had an intense brown color characteristic of the presence of the [2Fe–2S] cluster, indicating remarkably improved stability of the mutated T4moC after removal of Cys84 and Cys85. The crystals belonged to space group $C222_1$, with unit-cell parameters a = 44.360, b = 52.530, c = 83.490 Å.

3.3. Structure determination

The structure of T4moC was solved to a resolution of 1.48 Å. Table 1 shows data-collection, processing and refinement statistics. Previous studies have shown that the bacterial expression host removed Met1 (Skjeldal *et al.*, 2004). No electron density was observed for His111 and Ser112, which were present according to mass-spectrometric analysis. The final structure was refined to include 996 non-H atoms from the protein. The [2Fe–2S] cluster was observed with full occupancy. In addition, two other metal atoms with octahedral coordination were identified nearest to Ser53 O and to the carboxyl groups of Asp96 and Asp97. These atoms were assigned to be Mg based on its presence in the crystallization buffer. Three ethylene glycol molecules and 133 water molecules were also identified and included in the refinement. The final R value and free R value were 0.156 and 0.176, respectively, for 16 626 unique reflections observed between 33.92 and 1.48 Å (99.9% completeness). Ramachandran analysis and the r.m.s. deviations in bond lengths and bond angles are also presented in Table 1. All φ and ψ angles were in the most favored or additionally allowed regions; the average deviations in bond lengths and bond angles were 0.02 and 2.427 Å, respectively. Pro81 was observed in the *cis* configuration, as for the proline residues in the comparable primary sequence position in other Rieske proteins. The side chains of Lys39, Pro90 and Val100 showed two configurations with occupancies of 0.65 and 0.35.

The overall structure exhibited a mean B value of ∼14 Å^2. Examination of individual anisotropic B values indicated that T4moC was well folded in the region around the Cys84Ala and Cys85Ala mutations. A spherical depression that approximates the van der Waals radius of sulfur is found adjacent to Trp69 and the methyl group of Ala84. This depression is occupied by water in the crystal structure. Therefore, it is possible that Cys84 SG would occupy this depression and be partly exposed to solvent in the native enzyme. Moreover, the methyl group of Ala85 is exposed to solvent, suggesting that Cys85 SG would also be exposed to solvent in the natural protein. As the ability of O_2^- to destroy [2Fe–2S] clusters is known (Flint *et al.*, 1993), it is conceivable that the exposed thiol groups of Cys84 and Cys85 may become involved in an adventitious generation of reactive oxygen species over the long time period of crystallization trials.

Fig. 2 shows a ribbon diagram of T4moC. The protein consists of a β-sheet subdomain and a metal-binding subdomain. The [2Fe–2S] cluster is buried within the protein and has tetrahedral coordination completed by SG from Cys45 and Cys64 and ND1 from His47 and His67. The NE1 atoms of both His47 and His67 are solvent-exposed. A *VAST* search revealed that T4moC aligned best with the following Rieske proteins: the Rieske-type ferredoxin BphF from the *cis*-dihydrodiol-forming enzyme biphenyl dioxygenase (r.m.s.d. 1.222 Å; PDB code 1fqt; Colbert *et al.*, 2000), arsenite oxidase (r.m.s.d. 1.556 Å, PDB code 1g8j; Ellis *et al.*, 2001), carbazole 1,9a-dioxygenase ferredoxin (CarAc; r.m.s.d. 2.096 Å, PDB code 1vck; Nam *et al.*, 2005), the *Thermus thermophilus* Rieske protein (r.m.s.d. 5.014 Å, PDB code 1nyk; Hunsicker-Wang *et al.*, 2003) and Rieske ferredoxin subdomain of naphthalene dioxygenase (r.m.s.d. 8.763 Å, PDB code 1ndo; Kauppi *et al.*, 1998). Thus, T4moC is most similar to BphF, which is consistent with the known function of these two proteins as intermediate electron carriers for multiprotein oxygenase complexes.

3.4. Positioning of [2Fe–2S], Trp69 and Pro81

Nearly all Rieske ferredoxins contain a prolyl residue in the *cis* configuration (corresponding to Pro81 of T4moC) that helps to produce a loop near to the [2Fe–2S] cluster. In BphF, this residue is Pro82, which lies within ∼4 Å of the [2Fe–2S] cluster, a distance constraint that is typical of both Rieske ferredoxins and most Rieske-type ferredoxins.

Fig. 3(*a*) shows another difference between the structures of T4moC and BphF, in which although the loop containing Pro81 in T4moC is the same size as the loop containing Pro82 in BphF, it has been displaced ∼8 Å away from the [2Fe–2S] cluster by the presence of the Trp69 side chain. Since all the diiron hydroxylase ferredoxins shown in Fig. 1 also have a tryptophan residue in the primary sequence position corresponding to Trp69 of T4moC, it is likely that this entire clade will have this structural feature. In contrast, none of the other dioxygenase ferredoxins shown in Fig. 1 have a tryptophan residue at this position, but instead have glycine or alanine at this position (Nam *et al.*, 2005), suggesting their structures will be most comparable to those of BphF and CarAc.

Fig. 3(*b*) shows details of the interaction of Trp69 with the [2Fe–2S] cluster in T4moC. One bridging sulfide makes close contacts with Trp69 N (3.66 Å), Trp69 NE1 (3.86 Å) and Trp69 CD1 (3.34 Å), while Trp69 CZ2 is 3.66 Å from His67 CD2. A similar placement of a tryptophan side chain adjacent to the [2Fe–2S] cluster is observed in naphthalene dioxygenase (Kauppi *et al.*, 1998) and predicted from the primary sequences of most other *cis*-dihydrodiol-forming dioxygenases (Nam *et al.*, 2005; Martins *et al.*, 2005).

3.5. Hydrogen bonding to the [2Fe–2S] cluster

The loop-size analysis developed by Hunsicker-Wang and coworkers has been correlated with the number and identity of hydrogen bonds observed to the [2Fe–2S] cluster core across the broader group of Rieske and Rieske-type ferredoxins (Hunsicker-Wang *et al.*, 2003).

Fig. 4 shows that T4moC has five hydrogen bonds to the S atoms of the [2Fe–2S] cluster and the Cys ligands based on the

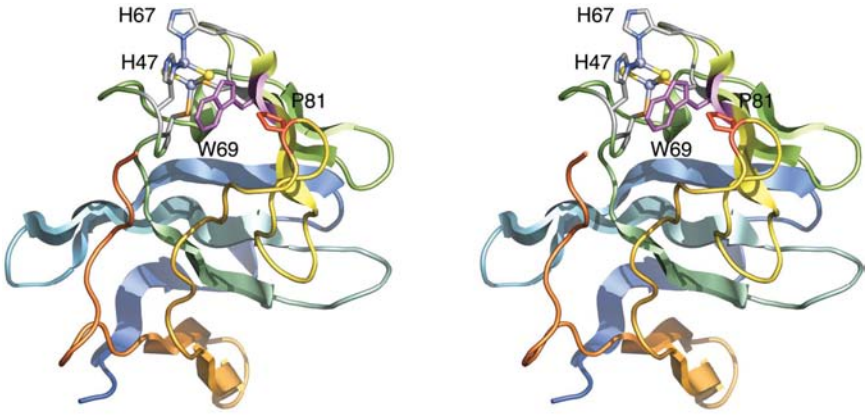

Figure 2
Stereo representation of the T4moC ribbon structure annotated with the positions of the [2Fe–2S] cluster, the ligands His47 and His67, Trp69 (purple) and Pro81 (red). The protein chain is colored from blue at the N-terminus to red at the C-terminus.

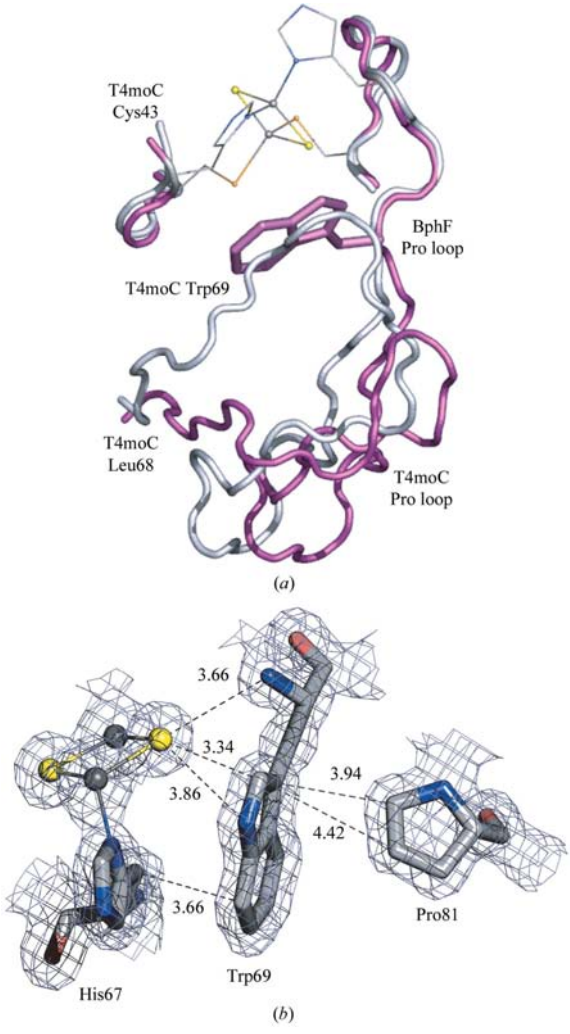

Figure 3
(*a*) Alignment of T4moC (purple, Cys45–His47 and Cys63–Leu86) and BphF (silver, Cys43–His45 and Cys63–Ala85) showing the overlap of the positions of Trp69 and the Pro loop of BphF. The Pro loop of T4moC is consequently displaced away from the [2Fe–2S] cluster by ∼8 Å. (*b*) Electron-density map with 2σ (grey) contouring of of T4moC showing the location of His67, Trp69 and Pro81 relative to the [2Fe–2S] cluster. Dotted lines show the distances between selected atoms.

criteria of a distance between the donor and acceptor atoms of 3.8 Å or less and a donor–proton–acceptor angle of 120–180° (Hunsicker-Wang *et al.*, 2003). Of these five, the N atoms of His47, Gln48, Ala66 and His67 were previously proposed from paramagnetic ^{15}N NMR studies (Xia *et al.*, 1998). The fifth hydrogen bond identified in the X-ray structure connects Trp69 N and a bridging sulfide atom (see Fig. 3*b*). Thus, the hydrogen-bonding pattern observed by X-ray crystallography also distinguishes T4moC from BphF, which has only three hydrogen bonds to the comparable S atoms (His45 NH to Cys43 SG, Leu65 NH to Cys63 SG and Gly68 NH to bridging sulfide) and $E^\circ \simeq -150$ mV. Related to BphF, Nam *et al.* (2005) showed that CarAc, with $E^\circ \simeq -167$ mV, has two hydrogen bonds to the cluster S atoms (His48 NH to Cys46 SG, Phe67 NH to Cys65 SG). Interestingly, a third putative hydrogen bond between Gly70 NH and a bridging inorganic sulfide has a distance of 3.9 Å and donor–proton–acceptor angle of 112°, just outside the above-mentioned geometric constraints. For comparison, the *T. thermophilus* Rieske protein has $E^\circ \simeq +150$ mV and seven hydrogen bonds (His134 NH and Tyr158 OH to Cys132 SG, Cys153 NH to Cys151 SG, His154 NH and Gly156 NH to S1 and Leu135 NH and Cys137 NH to S2; Zu *et al.*, 2003). The redox potential of T4moC is not known, but would be predicted (Zu *et al.*, 2003) to be between those of BphF and the *T. thermophilus* Rieske protein.

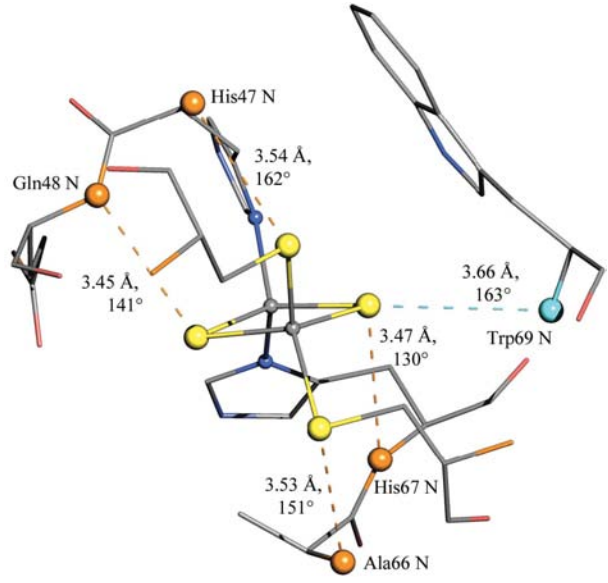

Figure 4
Hydrogen bonding to the S atoms of the [2Fe–2S] cluster in T4moC. The dotted lines show the distances between N and S atoms; distances and donor–proton–acceptor angles are derived from the X-ray structure. Hydrogen bonds involving the N atoms shown in orange are consistent with results of paramagnetic ^{15}N NMR studies (Xia *et al.*, 1998).

3.6. Electrostatic surface

Fig. 5 shows electrostatic surfaces of T4moC, TbuB, BphF and CarAc. TbuB is a closely related Rieske ferredoxin from the diiron clade (GenBank accession No. AAB09620.1; Fig. 1). Fig. 5(*a*) shows that T4moC is a highly acidic protein with a net charge of −14.2 and a large negatively charged patch (red) that extends along the groove separating the β-sheet subdomain and the metal-binding domain. T4moC also has a protruding basic patch provided by Arg65 that extends from the His ligands, particularly His67. A molecular threading of TbuB by *ESyPred3D* (Lambert *et al.*, 2002) using T4moC (PDB code 1vm9) as the target structure and subsequent electrostatic analysis (net charge of −11.2) revealed conservation of both the negatively charged patch and the surface Arg near to the His ligands (Fig. 5*b*). In contrast, Figs. 5(*c*) and 5(*d*) show that both BphF and CarAc lack the extent of the negatively charged surface (net charges of −8.3 and −6.2, respectively). Moreover, BphF lacks a prominent basic patch near to the [2Fe–2S] cluster, while CarAc has a basic patch in a different position relative to the [2Fe–2S] cluster than T4moC (Nam *et al.*, 2005). These differences support a contributing role of electrostatics in the specialization of complex formation in the different Rieske-type ferredoxin-dependent enzymes. Comparison of the upper right quadrants of the structures in Fig. 5 also reveals the steric differences caused by the placement of Trp69 against the [2Fe–2S] cluster in T4moC (Fig. 5*a*) compared with BphF (Fig. 5*c*) and CarAc (Fig. 5*d*).

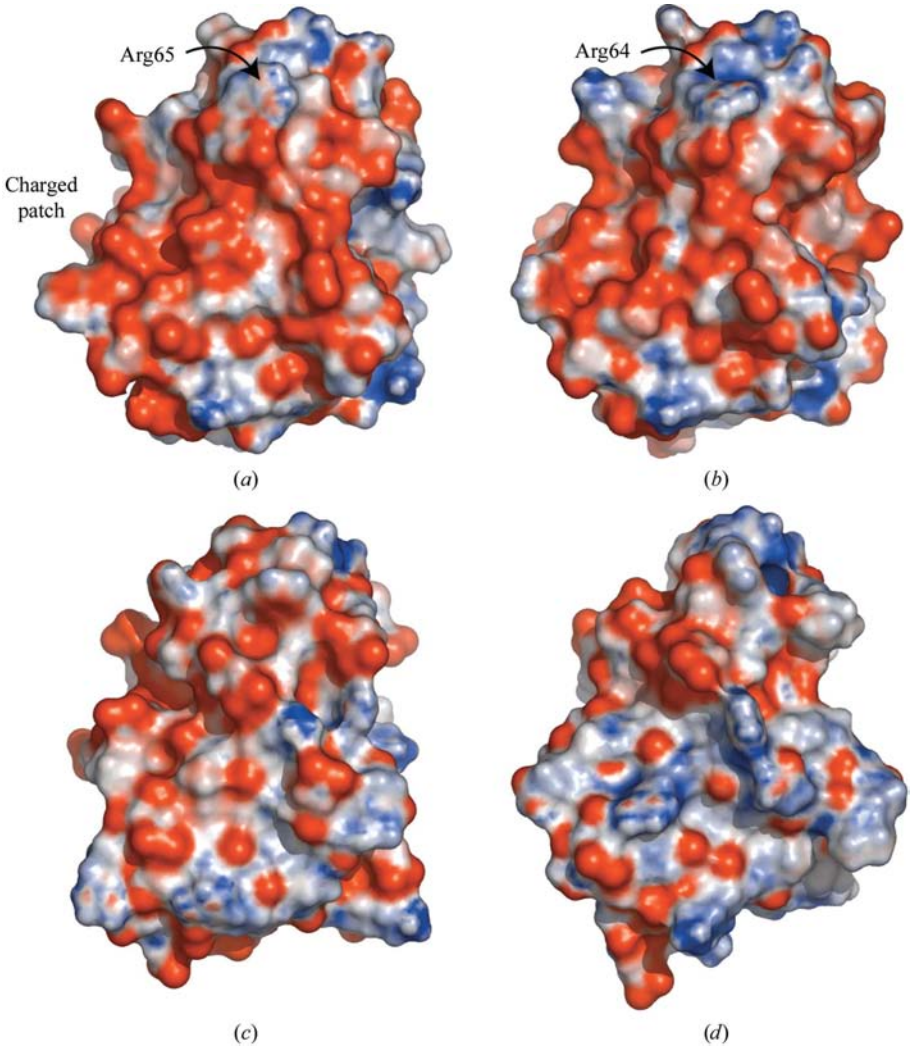

Figure 5
Electrostatic surfaces shown as a gradient from −10 keV/*T* (red) to +10 keV/*T* (blue). (*a*) The surface of T4moC, including the location of a large negatively charged patch at the central portion of the molecule and a basic patch including Arg65 adjacent to His67. Ala84 and Ala85 are located on the opposite surface of T4moC. (*b*) The predicted electrostatic surface of TbuB shown in the same orientation as T4moC after alignment of the [2Fe–2S] clusters and conserved ligands. (*c*) BphF shown in the same orientation as T4moC after alignment of the [2Fe–2S] clusters and conserved ligands. (*d*) CarAc shown in the same orientation as T4moC after alignment of the [2Fe–2S] clusters and conserved ligands.

3.7. Conclusion

The present X-ray structure reveals that T4moC has differences in the positioning of the protein backbone near to the [2Fe–2S] cluster, in the number of hydrogen bonds to the [2Fe–2S] cluster and in the electrostatic surface compared with BphF, its closest structural and functional homolog. Based on phylogenetic arguments, these differences are likely to be conserved in the Rieske-type ferredoxin components from the diiron monoxygenases and thus distinguish this clade from the comparable ferredoxins from the *cis*-dihydrodiol-forming aromatic dioxygenases. Whether any of these physical differences contribute to an often-assumed functional specialization of otherwise homologous proteins remains to be determined.

This work was funded by the National Science Foundation MCB-0316232 to BGF and by the Protein Structure Initiative of the National Institutes of Health P50 GM-64598 (John L. Markley, PI; GNP and BGF, Co-Investigators). Use of the Advanced Photon Source was supported by the US Department of Energy, Office of Science, Office of Basic Energy Sciences under Contract No. W-31-109-Eng-38. Access to APS station 32-ID-B was made possible by the LS-CAT user program. We thank LS-CAT beamline scientist Joe Brunzelle for facilitating data collection and David Smith and Simon Allard for their assistance with crystallization and data collection.

References

Altschul, S. F., Madden, T. L., Schaffer, A. A., Zhang, J., Zhang, Z., Miller, W. & Lipman, D. J. (1997). *Nucleic Acids Res.* **25**, 3389–3402.

Baker, N. A., Sept, D., Joseph, S., Holst, M. J. & McCammon, J. A. (2001). *Proc. Natl Acad. Sci. USA*, **98**, 10037–10041.

Batie, C. J., Ballou, D. P. & Correll, C. C. (1992). *Chemistry and Biochemistry of the Flavoenzymes*, Vol. 3, edited by F. Mueller, pp. 543–556. Boca Raton: CRC Press.

Berry, E. A., Guergovas-Kuras, M., Huang, L.-S. & Crofts, A. R. (2000). *Annu. Rev. Biochem.* **69**, 1005–1075.

Berry, E. A., Huang, L. S., Zhang, Z. & Kim, S.-H. (1999). *J. Bioeng. Biomembr.* **31**, 177–190.

Bonisch, H., Schmidt, C. L., Schafer, G. & Ladenstein, R. (2002). *J. Mol. Biol.* **319**, 791–805.

Brünger, A. T., Adams, P. D., Clore, G. M., DeLano, W. L., Gros, P., Grosse-Kunstleve, R. W., Jiang, J.-S., Kuszewski, J., Nilges, M., Pannu, N. S., Read, R. J., Rice, L. M., Simonson, T. & Warren, G. L. (1998). *Acta Cryst.* D**54**, 905–921.

Carrell, C. J., Zhang, H., Cramer, W. A. & Smith, J. L. (1997). *Structure*, **5**, 1613–1625.

Chen, J. *et al.* (2003). *Nucleic Acids Res.* **31**, 474–477.

Colbert, C. L., Couture, M. M., Eltis, L. D. & Bolin, J. T. (2000). *Structure Fold. Des.* **8**, 1267–1278.

Coufal, D. E., Blazyk, J., Whittington, D. A., Wu, W. W., Rosenzweig, A. C. & Lippard, S. J. (2000). *Eur. J. Biochem.* **267**, 2174–2185.

Ellis, P. J., Conrads, T., Hille, R. & Kuhn, P. (2001). *Structure*, **9**, 125–132.

Flint, D. H., Tuminello, J. F. & Emptage, M. H. (1993). *J. Biol. Chem.* **268**, 22369–22376.

Harborne, N. R., Griffiths, L., Busby, S. J. & Cole, J. A. (1992). *Mol. Microbiol.* **6**, 2805–2813.

Hemmi, H., Studts, J. M., Chae, Y. K., Song, J., Markley, J. L. & Fox, B. G. (2001). *Biochemistry*, **40**, 3512–3524.

Higgins, D. G., Thompson, J. D. & Gibson, T. J. (1996). *Methods Enzymol.* **266**, 383–402.

Holst, M. & Saied, F. (1995). *J. Comput. Chem.* **16**, 337–364.

Hunsicker-Wang, L. M., Heine, A., Chen, Y., Luna, E. P., Todaro, T., Zhang, Y. M., Williams, P. A., McRee, D. E., Hirst, J., Stout, C. D. & Fee, J. A. (2003). *Biochemistry*, **42**, 7303–7317.

Iwata, S., Saynovits, M., Link, T. A. & Michel, H. (1996). *Structure*, **4**, 567–579.

Kauppi, B., Lee, K., Carredano, E., Parales, R. E., Gibson, D. T., Eklund, H. & Ramaswamy, S. (1998). *Structure*, **6**, 571–586.

Lambert, C., Leonard, N., De Bolle, X. & Depiereux, E. (2002). *Bioinformatics*, **18**, 1250–1256.

Leahy, J. G., Batchelor, P. J. & Morcomb, S. M. (2003). *FEMS Microbiol. Rev.* **27**, 449–479.

McRee, D. E. (1999). *J. Struct. Biol.* **125**, 156–165.

Martins, B. M., Svetlitchnaia, T. & Dobbek, H. (2005). *Structure*, **13**, 817–824.

Mitchell, K. H., Studts, J. M. & Fox, B. G. (2002). *Biochemistry*, **41**, 3176–3188.

Murshudov, G. N., Vagin, A. A. & Dodson, E. J. (1997). *Acta Cryst.* D**53**, 240–255.

Nam, J.-W., Noguchi, H., Fujimoto, Z., Mizuno, H., Ashikawa, Y., Abo, M., Fushinobu, S., Kobashi, N., Wakagi, T., Iwata, K., Yoshida, T., Habe, H., Yamane, H., Omori, T. & Nojiri, H. (2005). *Proteins*, **58**, 779–789.

Nam, J. W., Nojiri, H., Yoshida, T., Habe, H., Yamane, H. & Omori, T. (2001). *Biosci. Biotechnol. Biochem.* **65**, 254–263.

Otwinowski, Z. & Minor, W. (1997). *Methods Enzymol.* **276**, 307–326.

Pikus, J. D., Studts, J. M., Achim, C., Kauffmann, K. E., Münck, E., Steffan, R. J., McClay, K. & Fox, B. G. (1996). *Biochemistry*, **35**, 9106–9119.

Skjeldal, L., Peterson, F. A., Doreleijers, J. F., Moe, L. A., Pikus, J. D., Volkman, B. F., Westler, W. M., Markley, J. L. & Fox, B. G. (2004). *J. Biol. Inorg. Chem.* **9**, 945–953.

Studts, J. M., Mitchell, K. H., Pikus, J. D., McClay, K., Steffan, R. J. & Fox, B. G. (2000). *Protein Expr. Purif.* **20**, 58–65.

Terwilliger, T. C. (2002). *Acta Cryst.* D**58**, 1937–1940.

Terwilliger, T. C. (2003). *Methods Enzymol.* **374**, 22–37.

Xia, B., Pikus, J. D., Xia, W., McClay, K., Steffan, R. J., Chae, Y. K., Westler, W. M., Markley, J. L. & Fox, B. G. (1998). *Biochemistry*, **38**, 727–739.

Yen, K.-M., Karl, M. R., Blatt, L. M., Simon, M. J., Winter, R. B., Fausset, P. R., Lu, H. S., Harcourt, A. A. & Chen, K. K. (1991). *J. Bacteriol.* **173**, 5315–5327.

Zu, Y., Couture, M. M.-J., Kolling, D. R. J., Crofts, A. R., Eltis, L. D., Fee, J. A. & Hirst, J. (2003). *Biochemistry*, **42**, 12400–12408.